AAS 14-321

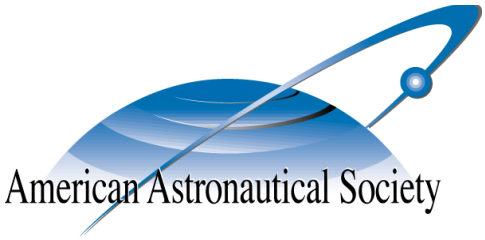



American Institute of
Aeronautics and Astronautics

# LONGITUDE-DEPENDENT EFFECTS OF FRAGMENTATION EVENTS IN THE GEOSYNCHRONOUS ORBIT REGIME

**Paul V. Anderson and Hanspeter Schaub**

**AAS/AIAA Space Flight Mechanics Meeting**

**Santa Fe, NM** **January 26 - 30, 2014**

**AAS Publications Office, P.O. Box 28130, San Diego, CA 92198**

AAS 14-321

# LONGITUDE-DEPENDENT EFFECTS OF FRAGMENTATION EVENTS IN THE GEOSYNCHRONOUS ORBIT REGIME

**Paul V. Anderson*** **and Hanspeter Schaub†**

The effects of on-orbit fragmentation events on localized debris congestion in each of the longitude slots of the geostationary (GEO) regime are evaluated by simulating explosions and collisions of uncontrolled rocket bodies in multiple orbit configurations, including libration about one or both of the gravitational wells located at 75°E and 105°W. Fragmentation distributions are constructed with the NASA Standard Breakup Model, which samples the area-to-mass ratio and delta-velocity as a function of effective diameter. Simulation results indicate that the long-term severity of the fragmentation event is strongly dependent upon parent body longitude at the epoch of fragmentation, which can spawn bi-annual "debris storms" in high-risk longitude slots, driven by fragments captured by the nearby gravity well.

## INTRODUCTION

The geostationary (GEO) regime is a unique commodity of the terrestrial satellite industry that is becoming increasingly contaminated with orbital debris,[1,2] but is heavily populated with high-value assets.[3] As the lack of atmospheric drag effects at the GEO altitude renders the lifetimes of these debris essentially infinitely long, conjunction assessment must be performed to safeguard operational GEO satellites from potential collisions with the uncontrolled population. GEO assets must maintain a specific longitude slot, and cannot simply phase shift to evade debris – thereby, analyses of the macroscopic behavior of the GEO debris population are required to describe debris fluxes through particular GEO longitude slots, and forecast how frequently operational satellites in these regions must potentially perform maneuvers to mitigate conjunctions. Of critical importance is a thorough understanding of the consequences that on-orbit object explosions and debris-debris or debris-asset collisions—collectively classified as *fragmentation events*—have on longitude-dependent congestion in the GEO regime. This knowledge is especially relevant, since although two historical fragmentation events have been documented at GEO (the 1978 explosion of the Ekran-2 satellite, and the 1992 explosion of a Titan III-C transtage[4]), significant populations of objects with diameters as small as 10-15 cm have been detected in optical observations of the GEO ring and are indicative of undetected fragmentation events in this arena.[4,5,6] On-orbit fragmentation is triggered by accidental mixing of hypergolic fuels, overheating of residual (non-vented) propellants, mechanical valve failures, hypervelocity impacts, or unknown means.[7] Recently, Reference 8 highlights that although a variety of work in the literature has been devoted to understanding debris cloud evolution in LEO, little research has been geared towards understanding fragmentation events at the GEO altitude, and

*Graduate Research Assistant, Department of Aerospace Engineering Sciences, University of Colorado Boulder, Boulder, CO, 80309.

†Professor, Department of Aerospace Engineering Sciences, University of Colorado Boulder, 429 UCB, Boulder, CO, 80309.

assessing the impact on the "background" debris congestion in this regime. Reference 12 highlights that understanding the effects of GEO fragmentations is a fruitful research area, especially since the kinetic energy distribution for GEO fragments is sufficient to penetrate orbit regimes from re-entry through super-synchronous. In addition to hindering the high-value services of operational assets, a GEO fragmentation event and the effects thereof might engender political repercussions as well.[12]

Forecasting of longitude-dependent congestion—termed debris weather—is imperative for space situational awareness activities in the GEO ring, as it provides a metric to gauge how frequently operators with assets in particular longitude slots will have to track nearby debris motion and consider executing avoidance maneuvers. Following Reference 9, this study harnesses a toroidal cell configuration at the GEO altitude to investigate the differing effects of a variety of simulated fragmentation events in this regime. The fragmentation particles are generated with the NASA Standard Breakup Model,[10] which has been validated against catalogued debris clouds and ground-based experimental results for particles larger than 1 mm.[4] This empirical model statistically samples the area-to-mass ratio and corresponding $\Delta v$ imparted to each particle at the fragmentation epoch, which is applied along a randomly-sampled unit vector and summed with the parent body's velocity vector. The torus intersection metric is then harnessed in tandem with a parallel propagation routine that implements $4 \times 4$ EGM-96 gravitation, luni-solar perturbations, and a cannonball solar radiation pressure model to evaluate longitude-dependent debris weather generated from the simulated fragmentation. It is of interest to note that depending on *where* the parent body is located at the fragmentation epoch, and *what* orbit class the parent body is categorized as, the longitude-dependent effects of the explosion or collision may be more or less severe for operational assets in high-risk longitude slots, especially those near the debris-critical gravitational wells located at 75°E and 105°W.

On-orbit fragmentation in the GEO regime has the potential to create significant localized congestion, dependent not only upon the altitude at break-up, but the longitude at which the fragmentation occurs. Explosions of lower-energy, librating objects over one of the two gravitational wells spawn bi-annual debris storms that threaten the safety of operational assets stationed in longitude slots near these debris-critical regions. This paper fills a critical void in the literature by addressing fragmentation events in the delicate GEO regime from the perspective of the rotating, Earth-fixed frame, and not inertial space, which has typically been utilized for fragmentation studies in both the LEO and GEO regimes (see References 11-12, for example). On-orbit fragmentation for a variety of different break-up scenarios is simulated to rapidly investigate short- and long-term contributions to nominal, baseline congestion occurring on a localized basis for each of the GEO longitude slots. As the debris population continues to increase—especially as a result of on-orbit fragmentations—the amount of propellant required to maintain a specified longitude slot while simultaneously executing avoidance maneuvers, and the costs associated with analyzing conjunction events to discern if evasive action is even necessary, will begin increasing in tandem. From the new perspective illustrated by this paper, the significance of fragmentation events on GEO longitude slot safety will be cast in a new light to impel further research in this critical area.

## METHODOLOGY FOR FORECASTING LOCALIZED CONGESTION

### Overview of Near-Miss Events Metric

Near-miss events for the GEO longitude slots are determined by formulating a GEO-encompassing torus of major radius $r_{\text{GEO}} = 42164$ km and minor radius $\tilde{r}$, partitioned into longitude increments of $\Delta\lambda = 1.0^{\circ}$.[9] The minor radius $\tilde{r}$ is equivalent to the radius of the circular torus cross-section, and provides a means to evaluate debris congestion levels occurring within various distances of the GEO

longitude slots; a larger minor radius captures more near-miss events. In this study, a representative minor radius of $\tilde{r} = 100$ km is considered, as this radius provides a rough upper bound for distances at which precise conjunction assessment could be considered for GEO satellites. Further, this torus formulation is a natural choice for detecting near-miss events for the non-inertial longitude slots, as torus geometry is invariant as seen by both the inertial frame (i.e., MJ2000) and the Earth-centered, Earth-fixed frame, in which the GEO longitude slots are stationary.[9]

Near-miss events are detected during propagation of an object by checking for the transversal of this GEO torus boundary at each time step during numerical integration; if finer resolution is desired, an interpolation scheme can implemented to check for torus intersections between integration time steps. Mathematically, a near-miss event occurs if[9]

$$\left(r_{\text{GEO}} - \sqrt{r_X^2 + r_Y^2}\right)^2 + r_Z^2 - \tilde{r}^2 < 0 \tag{1}$$

is satisfied, where $(r_X, r_Y, r_Z)^T$ is the RSO position vector expressed in inertial frame components. The longitude of intersection $\lambda_{\text{CPE}}$ is thus determined as:

$$\lambda_{\text{CPE}} = \arctan\left(\frac{r_Y}{r_X}\right) - \alpha_G \tag{2}$$

where $\alpha_G$ is the right ascension of Greenwich (Greenwich sidereal time).[13] When a torus-intersection is detected with Equation (1), the longitude of intersection is determined with Equation (2), and the total near-miss event count for the associated torus cell is updated. To ensure that equivalent intersections are not accounted for more than once during event checking, counting logic is implemented before a cell intersection counter is updated to screen the event for redundancy. The full algorithm for quantifying congestion via near-miss events with the torus formulation is detailed in Reference 9.

**Propagator and Implementation**

A special perturbations propagation routine implemented in ANSI-C and parallelized with OpenCL is utilized to propagate explosion/collision fragments forward in time and quantify torus intersection events.* A lower-fidelity, representative force model of the GEO environment is used for the added benefit of dramatically-decreased simulation run times. Here, the two-body equations of motion are numerically integrated under $4 \times 4$ EGM-96 gravitation, luni-solar perturbations, and solar radiation pressure (SRP), modeled with the cannonball assumption described in Reference 14, and attenuated with the occultation algorithm presented in Reference 15. The equations of motion are

$$\ddot{\boldsymbol{r}} = -\frac{\mu_\oplus}{r^3}\boldsymbol{r} + \boldsymbol{a}_\oplus + \boldsymbol{a}_{\leftmoon} + \boldsymbol{a}_\odot + \boldsymbol{a}_{\text{SRP}} \tag{3}$$

where the first term denotes two-body acceleration, $\boldsymbol{a}_\oplus$ is the acceleration due to the nonsphericity of Earth, $\boldsymbol{a}_{\leftmoon}$ and $\boldsymbol{a}_\odot$ are the third-body perturbations from the Moon and Sun, respectively, and $\boldsymbol{a}_{\text{SRP}}$ is the SRP acceleration. SRP is modeled using the inverse-square diffusion formulation of the solar luminosity $L_\odot \approx 3.839 \times 10^{26}$ J/s, with coefficient of reflectivity $c_r \equiv 1.5$ and area-to-mass ratio $A_\odot/m$ sampled in the NASA Standard Breakup Model, as discussed below. This GEO force model is in agreement with the results of Reference 8, which ranks the importance of incorporating various environmental perturbations in GEO force models for debris analysis over time scales ranging from

**OpenCL 1.2 Specification* is available from Khronos Group at: `http://www.khronos.org/registry/cl/`.

1 week to 10 years. This study treats fragmentation-induced congestion over at least a 5-year period, a time scale over which luni-solar perturbations become especially relevant for uncontrolled debris objects at GEO.

In higher-fidelity force models, coordinate transformations between Earth-fixed and Earth-inertial frames utilize accurate Earth orientation parameters to account for precession, nutation, and polar motion; software suites such as the SPICE toolkit can be harnessed to perform these complex coordinate transformations.* In this parallelized propagator, however, a lower-fidelity transformation that accounts strictly for a $z$-axis rotation by Greenwich sidereal time is used for purposes of increased speed at run time. Furthermore, instead of extracting inertial Moon and Sun position vectors from the DE-421 ephemerides, this routine implements low-precision formulae for the geocentric coordinates of these bodies, as provided in the 2013 *Astronomical Almanac*.[17] Reference 18 validates this lower-fidelity force model by comparing simulation results over a 5-year period with those obtained using a higher-fidelity force model. Since debris congestion results equivalent to those presented in the current paper change insignificantly when higher-fidelity forcing is used, lower-fidelity, parallel propagation is harnessed for the dramatic speed increase it provides.

The propagator utilizes an eighth-order, predictor-corrector Gauss-Jackson integrator[19] initialized with the Prince-Dormand 8(7) algorithm for integration of the equations of motion in Equation (3). For near-miss event computations during the congestion forecast, a time step of 1 minute is specified for sufficient fidelity in capturing macroscopic congestion trends. To enhance the resolution without significantly increasing run times, linear interpolation is used to check for torus intersections in 6 sec increments between primary time steps. Linear interpolation is an appropriate assumption in this case, because an object in a two-body GEO orbit will move through a circular arc of $\theta_{\text{arc}} \approx 0.25^\circ$ in one minute, such that at the GEO altitude, the straight-line approximation over this time span will only deviate from the true curvilinear orbit by approximately $r_{\text{GEO}}\left[1 - \cos(\theta_{\text{arc}}/2)\right] \approx 0.1$ km at maximum, based upon the geometry of circular segments. Since the GEO torus considered here has a minor radius of 100 km, this discrepancy does not affect the resolution of the congestion forecast.

**Fragmentation Model**

In this study, fragmentation particulates are generated using the NASA Standard Breakup Model, developed for NASA's long-term debris environment software EVOLVE 4.0,[10] and validated against catalogued debris clouds and ground-based experimental results for particles larger than 1 mm.[4] The NASA model uses an empirical power law to determine the cumulative number of fragments larger than a user-defined effective diameter $l_c$. For explosions, the cumulative number of fragments $N_f$ is

$$N_f(d \geqslant l_c) = 6 c_s l_c^{-1.6} \tag{4}$$

where $d$ denotes fragment diameter, $l_c$ is the defined effective diameter in meters, and $c_s$ is a unitless, empirical correction for catalogued fragmentation events.[4] For this study, the correction $c_s = 1.0$ is assumed.† For collisions, $N_f$ is a function of the target and impactor masses and collision velocity:[4]

$$N_f(d \geqslant l_c) = 0.1 \hat{m}^{0.75} l_c^{-1.71} \tag{5}$$

*NASA/JPL's SPICE toolkits are available at: `http://naif.jpl.nasa.gov/naif/toolkit.html`.

†Reference 10 states that this relationship is valid for launch vehicle upper stages with masses of 600-1000 kg, and introduces the correction factor to account for known debris from catalogued explosions of other parent body masses/types.

where the mass-dependent factor $\hat{m}$ is defined as

$$\hat{m} \equiv \begin{cases} m_t + m_p \text{ [kg]} & \text{for } \tilde{E}_p \geqslant \tilde{E}_p^* \quad \text{[catastrophic]} \\ (m_p v_i)/1000 \text{ [kg m/s]} & \text{for } \tilde{E}_p < \tilde{E}_p^* \quad \text{[non-catastrophic]} \end{cases} \tag{6}$$

where $m_t$ and $m_p$ denote the target and impactor masses, $v_i$ is the magnitude of the impact velocity, $\tilde{E}_p$ is the specific energy of the impactor, defined as $\tilde{E}_p = 0.5 m_p v_i^2 / m_t$, and $\tilde{E}_p^* \equiv 40$ kJ/kg is the energy threshold for a catastrophic collision.[4] For effective diameters $l_c > 11$ cm, a bi-modal probability distribution is used to sample the area-to-mass ratio for every fragment. For $l_c < 8.0$ cm for spacecraft fragments, and $l_c < 1.7$ cm for upper stage fragments, a single-mode normal distribution is employed.[4] For effective diameters within the definition gap of 8-11 cm for spacecraft and 1.7-11 cm for upper stages, a pseudo-random number on [0,1] is generated to determine if the bi-modal or single-mode distribution should be utilized.[4] The cross-sectional area for each fragment is then determined as an explicit function of the effective diameter $l_c$, and the fragmentation "delta-velocity" applied to the fragment is sampled from a normal distribution on the area-to-mass ratio.[10] Figure 1 illustrates a flow-chart for using the NASA model – for more details regarding implementation, and the parameters utilized in the bi-modal and single-mode area-to-mass ratio and velocity distributions in the model, the reader is referred to References 4 and 10. Note that for explosions and collisions, the delta-velocity is applied in a random direction for each fragment, sampled over the unit sphere. The number of fragments in each debris cloud resulting from a collision event is proportional to the mass fractions of the target and impactor, i.e., given $m_t = m_p$, each cloud receives $0.5 N_f$ fragments.

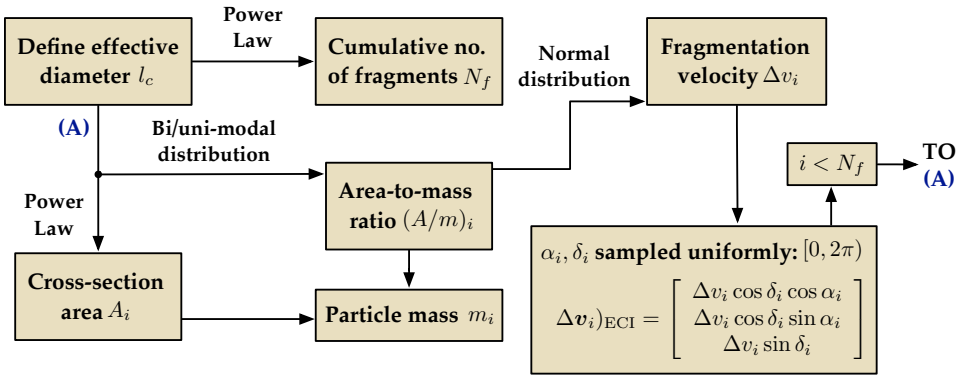


**Figure 1. Flow-chart for computer implementation of NASA Standard Breakup Model.**

## BACKGROUND NOISE FROM CURRENT DEBRIS POPULATION

The object population in the GEO arena is classified with a taxonomy used by the European Space Agency's DISCOS database (Database and Information System Characterising Objects in Space).[20] For GEO objects, seven orbit categories are selected to classify the type of orbits traversed by these objects. Table 1 gives a description of this classification system – note that only uncontrolled objects are assumed to contribute to localized congestion in this study. GEO objects are selected according to the requirements imposed in the ESA *Classification of Geosynchronous Objects* reports:[20]

- Eccentricity smaller than 0.2 ($e < 0.2$)

- Inclination smaller than $70^\circ$ ($i < 70^\circ$)
- Mean motion between $0.9$ and $1.1$ revolutions per sidereal day ($0.9 < n < 1.1$)*

**Table 1. Orbit classifications for geosynchronous objects used in GEO congestion study.**

| Class | Type | Description |
|---|---|---|
| C1 | Controlled | Longitude/inclination control (E-W/N-S control) |
| C2 | Controlled | Longitude control only (E-W control only) |
| D | Drifting | Drift above/below/through protected GEO zone |
| L1 | Librating | Libration about Eastern stable point ($\lambda = 75^\circ$E) |
| L2 | Librating | Libration about Western stable point ($\lambda = 105^\circ$W) |
| L3 | Librating | Libration about Eastern/Western stable points |
| IN | Indeterminate | Unknown status (e.g., recent TLE not available) |

Orbital data are obtained from publicly-available two-line element (TLE) sets provided by U.S. Strategic Command (USSTRATCOM).† For this study, a reference TLE set obtained on 08/28/2013 is used. TLE data are given in the form of doubly-averaged Keplerian elements with mean motion instead of semi-major axis,[4] transformed into Cartesian states within the true equator, mean equinox (TEME) frame[14] with SGP-4 theory.[21]‡ Note that because of the limited accuracy of the TLE sets, these data are not intended for studies that require highly-precise orbit prediction capabilities. As the purpose of this paper is to forecast localized debris congestion generated by on-orbit fragmentation events on a macroscopic scale, the accuracy of these data is sufficient for this baseline "background noise" assessment. Furthermore, as only objects larger than approximately 0.8-1.0 meter in effective diameter are actively tracked at the GEO altitude,[20] only objects at least of this size are considered in the background noise forecast.

As a precursor to identifying the longitude-dependent effects of fragmentations at GEO, a 5-year macroscopic congestion forecast is performed with the minor radius $\tilde{r} = 100$ km, using the baseline object population in the 08/28/2013 TLE set to evaluate current levels of background noise in this regime. Controlled assets (C1/C2) are assumed to maintain their specified longitude slots, while the 750 uncontrolled GEO objects from this set are propagated forward in time and incorporated in the near-miss study. Note that this simulation is only assessing the congestion generated by the current debris population over a 5-year time frame. Nominal population growth,§ solid rocket motor (SRM) slag, multi-layered insulation (MLI) shedding, and other debris growth mechanisms considered in Reference 23, for example, are not treated in this simulation. The debris weather forecast for GEO for this 5-year period is shown in Figure 2, which illustrates the number of near-miss events *per day* at 100 km for each of the longitude slots at GEO. Accumulation of uncontrolled objects around the gravitational wells at 75°E and 105°W is a well-known result, as is discussed in References 24-25. This is a particularly troublesome notion, as operational assets are typically inserted into longitude slots near the gravitational wells,[18] and the probability of collision in the vicinity of the gravitational wells is seven times larger than in surrounding regions at GEO.[3,26] From Figure 2, controlled assets

*This mean motion range corresponds to the semi-major axis range $[-2596, 3068]$ km with respect to the GEO radius.

†Publicly-available TLE data sets are available for bulk download from `https://www.space-track.org/`

‡ANSI-C implementation of merged SGP-4/SDP-4 theory is available from `http://www.sat.dundee.ac.uk/~psc/sgp4.html`[22]

§The effect of nominal launch traffic on longitude-dependent congestion at GEO is simulated in Reference 18.

in the longitude slots neighboring the gravitational wells are subject to 6-10 "close calls" per day at a miss distance of 100 km – this is on-par with the factor of seven increase over the less congested regions (e.g., Atlantic/Pacific Oceans), which experience a maximum of 1-2 near-misses per day at this distance. Since this congestion forecast only includes the trackable, catalogued, and unclassified GEO objects with up-to-date TLEs, these results serve to illustrate the conservative lower bound of the actual debris background noise in the GEO ring.

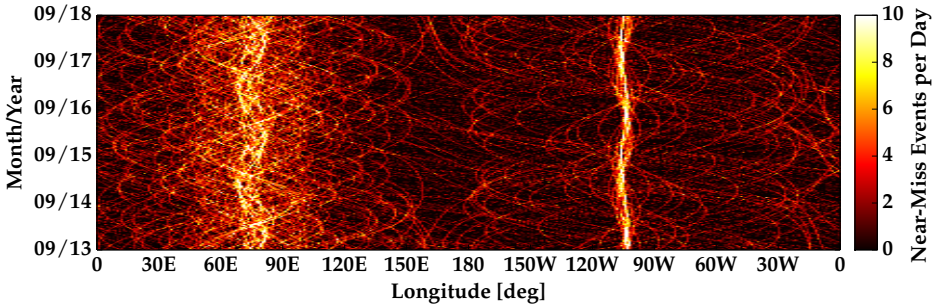


**Figure 2. Five-year localized debris congestion forecast at GEO (100 km torus).**

## LONGITUDE-DEPENDENT EFFECTS OF FRAGMENTATIONS AT GEO

The longitude-dependent congestion generated by fragmentation of a rocket body (R/B) over one of the gravitational wells at 75°E and 105°W may be characterized by applying the NASA Standard Breakup Model to a simulated R/B positioned at various longitudes in GEO orbit. Reference 8 states that a lower-energy fragmentation over one of the gravitational wells could be a worst-case scenario in that resonance is preserved for a majority of the fragments generated in the breakup, resulting in frequent near-misses with operational assets in the vicinity of these critical longitudes. The results of this current study will illustrate that this hypothesis in Reference 8 is precisely the case – not only does longitude-dependent congestion increase as a function of the number of fragments "captured" by the gravitational well, but these localized congestion increases are predictable to first-order both in longitude and time since breakup. First, we consider the theory introduced in Reference 27, which provides the mathematics necessary for predicting libration parameters based upon initial longitude and longitudinal drift rate – these parameters are combined with a harmonic oscillator model to give a first-order, analytic formulation for the libration motion of fragments captured by the gravity well.

### Harmonic Oscillator Model of Libration Motion

Employing a change of origin $\psi \equiv \lambda - \lambda_{1,2}$, where $\lambda$ and $\lambda_{1,2}$ denote geocentric longitude of the object and gravitational well, respectively, the condition for stable point "capture" is expressed as[27]

$$\|\dot{\psi}_0\| < k\|\cos\psi_0\| \tag{7}$$

where $\dot{\psi}_0 = n_0 - n_{\text{GEO}}$ is the initial longitudinal drift rate (a function of the semi-major axis only), and $k$ is an angular-velocity-like parameter dependent upon the $J_{2,2}$ sectorial harmonic, defined as[27]

$$k \equiv \frac{6n_{\text{GEO}}R_{\oplus}\sqrt{J_{2,2}}}{r_{\text{GEO}}} \tag{8}$$

Utilizing the coefficient $J_{2,2} \approx 1.82 \times 10^{-6}$ derived from the EGM-96 gravity model,* the parameter $k \approx 8.92 \times 10^{-8}$ rad/s.[4] Following Reference 27, the amplitude and period of libration for objects that satisfy the capture condition given by Equation (7) are approximated with the two formulations

$$\sin \psi_m = \sqrt{\sin^2 \psi_0 + \frac{\dot{\psi}_0^2}{k^2}} \tag{9}$$

$$T_l = \frac{4}{k} K(\sin \psi_m) \tag{10}$$

where $\psi_m$ denotes the libration amplitude, $T_l$ is the period of libration, and $K(\sin \psi_m)$ is the complete elliptic integral of the first kind.[27] Note that Equations (9)-(10) are derived assuming the $J_{2,2}$ term only; higher-order harmonics appearing in a full expansion of the Earth gravitational potential are neglected. Therefore, since the propagator harnessed in this study uses a $4 \times 4$ gravitation model, Equations (9)-(10) provide a first-order approximation for the libration characteristics observed with numerical simulations. Nonetheless, these formulas can be used in tandem with a harmonic oscillator model to rapidly predict libration motion to first-order, i.e., under the $J_{2,2}$ perturbation alone. If an oscillatory solution is assumed, the longitudinal motion of a captured object can be expressed as

$$\lambda(t) = \psi_m \cos\left(\frac{2\pi t}{T_l} - \phi \operatorname{sgn}(\dot{\psi}_0)\right) + \lambda_{1,2} \tag{11}$$

where the phase shift $\phi$ is determined with

$$\phi = \arccos\left(\frac{\psi_0}{\psi_m}\right) \tag{12}$$

Note that the sign of the initial longitudinal drift rate $\dot{\psi}_0$ is included to switch the sign of the phase angle accordingly, such that the resulting sinusoidal longitude profile reflects the initial E/W drifting direction of the object. The accuracy of this harmonic oscillator model for predicting the resulting libration motion of fragments captured by a gravity well in the aftermath of fragmentation is explored in the following section, which assesses explosions in the neighborhoods of the critical stable points.

**Explosions over Gravitational Wells**

To investigate the localized debris congestion generated from explosions at the GEO altitude, the NASA Standard Breakup Model is applied to generate fragmentation debris with effective diameters $l_c > 5$ cm resulting from the explosion of a simulated R/B, with initial conditions that place the R/B at various longitudes surrounding the Eastern/Western gravitational wells at the simulated explosion epoch of midnight on 09/01/2013. From Equation (4), the NASA model forecasts that 724 fragments larger than 5 cm are generated in the explosion. The fragmentation $\Delta v$ for each fragment is applied in a random direction sampled over the unit sphere, which is added to the inertial velocity vector of the simulated R/B initial conditions $a = r_{\text{GEO}}$, $e = 0.001$, $i = \Omega = M_0 = 0^\circ$, with the argument of perigee $\omega$ chosen such that the R/B is positioned at the desired longitude, i.e., $\omega = \alpha_G + \lambda_0$, where $\alpha_G$ is the right ascension of Greenwich at the explosion epoch.[18] For the case $\lambda_0 = 60^\circ$E, Figure 3 illustrates the characteristics of the resulting fragment distribution. Figure 3(a) provides a Gabbard diagram that highlights the resulting perigee/apogee radius spread as a function of semi-major axis, normalized by the GEO radius, and Figure 3(b) shows the area-to-mass ratio and fragmentation $\Delta v$

*Coefficients for the EGM-96 model are available at: `http://cddis.nasa.gov/926/egm96/egm96.html`

distribution, colored by the capture metric in Equation (7). Note that 60 fragments are captured by the gravitational well at 75°E; of these, 57 are ejected at fragmentation delta-velocities less than 100 m/s, and 3 at fragmentation delta-velocities larger than 100 m/s, indicating that the direction of the fragmentation $\Delta v$ for these high-speed fragments is against the direction of the R/B velocity vector.

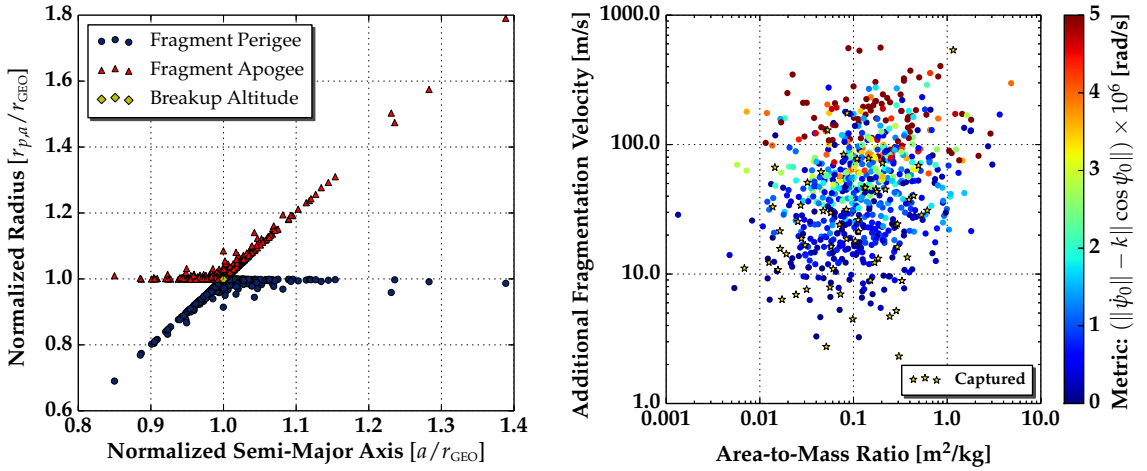


(a) Gabbard diagram for R/B explosion at 60°E.

(b) Fragment distribution for R/B explosion at 60°E.

**Figure 3. Characteristics of fragmentation distribution for simulated R/B explosion at 60°E.**

The five-year congestion forecasts for simulated R/B explosions occurring at 45°E, 60°E, and at the Eastern gravitational well at 75°E are illustrated in Figure 4 for a torus minor radius of $\tilde{r} = 100$ km. Note that 54, 60, and 69 of the 724 ejected fragments are captured by the Eastern gravitational well in each case, respectively, and begin librating around this critical longitude. As a consequence, bi-annual "debris storms," i.e., dramatic increases in localized congestion, occur at the longitudinal extents of the parent R/B's libration motion. This result is predicted by Equation (9), which indicates that $\psi_0 = \psi_m$ if $\dot{\psi}_0 = 0$, that is, the amplitude of the libration is equivalent to the initial deviation from the gravitational well inasmuch as $a = r_{\text{GEO}}$ at the explosion epoch. The congestion forecasts in Figure 4 illustrate that the resulting oscillations in longitude exhibited by the captured fragments synchronize in approximately one-year intervals at the libration amplitude of the parent R/B over the five-year prediction span. Therefore, this is critical knowledge not only for satellite operators with assets in longitude slots near the explosion longitude $\lambda_0$, but also for those with assets in longitude slots $2\psi_m$ away from $\lambda_0$ in the direction of the gravitational well. Note that the resulting background noise from the drifting fragments not captured by the gravitational well exhibits a yearly "banding" phenomenon driven by once-yearly oscillations in the eccentricity vector induced by SRP, the effects of which are more pronounced as a consequence of higher area-to-mass ratios (cf. Figure 3(b)).[28,29]

Figure 5 provides a zoomed-in, one-year view of the five-year congestion forecast in Figure 4(b). Curvilinear traces of the librating fragments captured by the gravitational well are clearly visible, in addition to the linear traces of the higher-energy fragments that evade capture and begin to circulate around the GEO ring with eastward drift for semi-major axes below the GEO altitude, and westward drift for semi-major axes above GEO.[9] Figure 6(a) illustrates the 60°E explosion case in Figure 4(b)

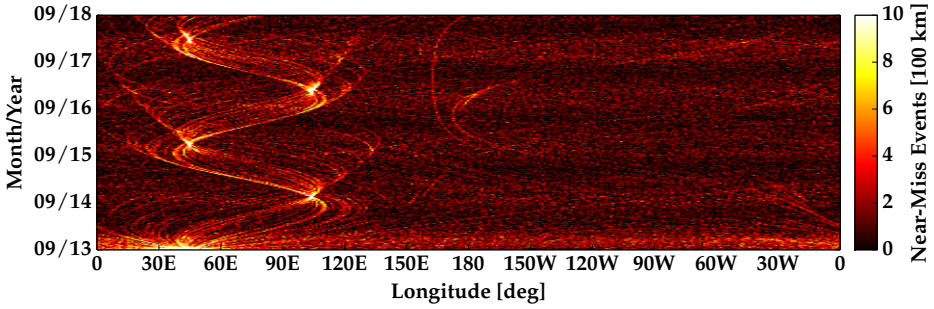


(a) Five-year congestion forecast for simulated R/B explosion at 45°E ($\tilde{r} = 100$ km).

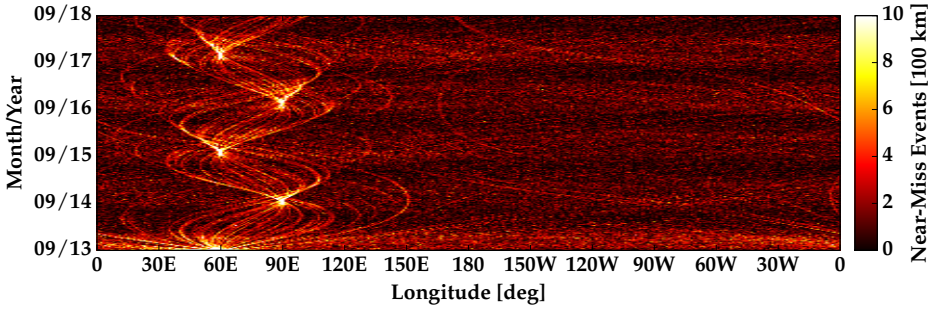


(b) Five-year congestion forecast for simulated R/B explosion at 60°E ($\tilde{r} = 100$ km).

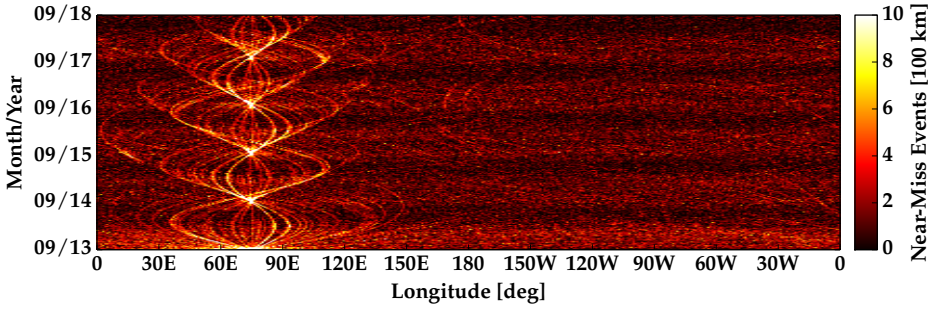


(c) Five-year congestion forecast for simulated R/B explosion at 75°E ($\tilde{r} = 100$ km).

**Figure 4. Longitude-dependent congestion from simulated R/B explosions near Eastern well.**

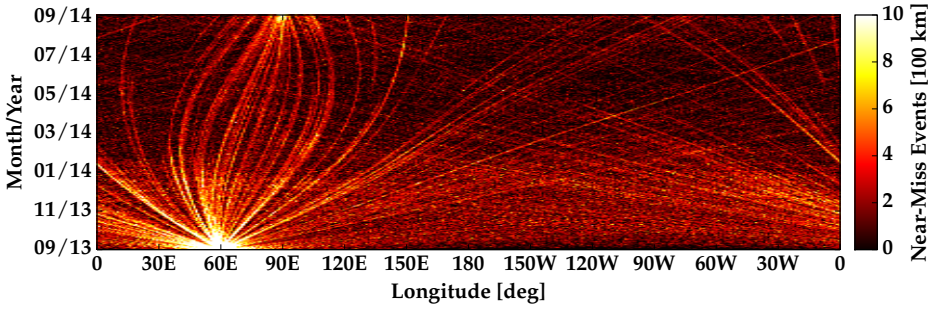


**Figure 5. Longitude-dependent congestion from simulated R/B explosion at 60°E (1 year).**

propagated for 30 years to illustrate localized congestion trends occurring over a longer time scale. Longitudinal focusing, although prominent for the first five years, begins to diffuse from 5-10 years, leading to a lull in the macroscopic debris weather from 10-20 years. From 20-25 years, the librating fragments begin refocusing into a characteristic oscillatory pattern – the intensity of these "residual" debris storms is beneath that observed in the first five years following the explosion, however. After 25 years, the librating fragments once again diffuse. Analysis of the simulation results indicates that the mechanism for this long-term focusing, diffusion, and re-focusing phenomenon is a combination of the long-period luni-solar effects and the SRP-induced eccentricity variations prevalent for GEO. If these perturbations are removed from the force model, such that the 30-year propagation considers $4 \times 4$ gravitation only, the localized congestion forecast in Figure 6(b) appears. In this situation, the fragment diffusion and re-focusing periods are not observed – rather, strong focusing at the libration amplitude persists throughout the entire 30-year simulation. This result emphasizes a conclusion of Reference 8 that luni-solar and SRP perturbations are critical for analyzing fragmentation events at GEO over durations longer than one year.

Figure 7 illustrates that similar focusing effects can occur for fragments captured by the Western gravitational well. For simulated R/B explosions at 75°W, 90°W, and at the Western gravitational well at 105°W, 58, 67, and 66 of the 724 ejected fragments are captured in each case, respectively. Note that although the number of captured fragments in each case is similar to the number captured in the Eastern well simulations illustrated in Figure 4, the intensities of the fragment focusing events are not as strong as the equivalent Eastern well cases, e.g., for $\psi_0 = 30^\circ$, cf. Figures 4(a) and 7(a). For completeness, Figure 8 illustrates the five-year congestion resulting from an explosion at 165°E, a well-known unstable equilibrium longitude located halfway between the stable gravitational wells. In this situation, none of the 724 ejected fragments are captured by either gravitational well via the metric in Equation (7); however, curvilinear traces in Figure 8 indicate that several fragments begin oscillating about both the gravitational wells, behavior indicative of L3 class objects (recall Table 1).

### Accuracy of Harmonic Oscillator Model

It is interesting to evaluate if the harmonic oscillator model in Equations (11)-(12) can sufficiently approximate the longitudinal "bunching" illustrated in the five-year congestion forecasts in Figure 4. Fragment focusing at the longitudinal extents appears predictable both in longitude and in time, such that a first-order model for forecasting these debris storms with minimal knowledge of the fragment distribution is desirable. If the semi-major axes $a_i$ for the resulting fragment orbits in the aftermath of a fragmentation can be reasonably estimated, $\dot{\psi}_{0,i}$ is a known initial condition, and Equations (9)-(10) can be harnessed to compute the amplitude and period of libration, respectively, for fragments captured via Equation (7). Longitude histories for these fragments are thus predicted analytically as a function of elapsed time with the model in Equations (11)-(12), and overlaid to forecast when and where fragment focusing will occur to first-order after a fragmentation event near the GEO altitude.

Figure 9 provides the accuracy of this harmonic oscillator model, showing comparisons between the analytical longitude histories predicted by the model in Figure 9(a), simulated longitude histories using the $J_{2,2}$ harmonic only in Figure 9(b), and simulated longitude histories using the full forcing model (i.e., $4 \times 4$ EGM-96 gravity, luni-solar perturbations, and SRP) in Figure 9(c). As anticipated, the harmonic oscillator approximation agrees well with the simulated longitudes under $J_{2,2}$ only, as this was the assumption made in the derivation of Equations (9)-(10). When compared against the "truth" longitude histories of the 60 librating fragments in Figure 9(c), however, discrepancies exist

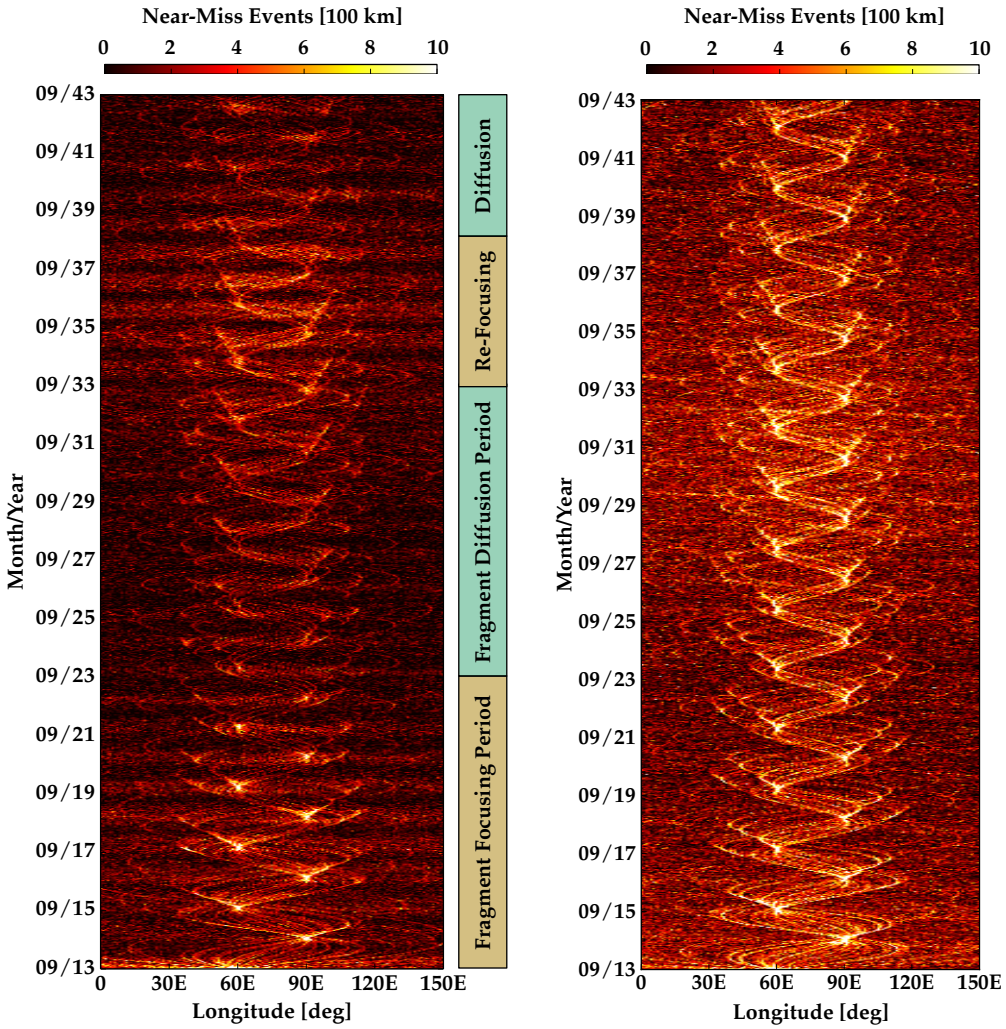


(a) Propagation under full forcing model.

(b) Propagation under $4 \times 4$ gravitation only.

**Figure 6. Longitude-dependent congestion from simulated R/B explosion at 60°E (30 years).**

not in the longitudinal location of the fragment focusing, but in the time that these focusing events occur. As this timing error increases with elapsed time since fragmentation, this harmonic oscillator model should only be employed for short-term, 1-2 year predictions. After this time span, dominant perturbations in the GEO environment that are not accounted for in the harmonic oscillator method begin influencing the libration motion of the fragments, and this $J_{2,2}$-only approximation diverges.

### Collisions over Gravitational Wells

Next, it is of interest to evaluate the longitude-dependent congestion signature of collision events in the GEO regime. Reference 8 indicates that since orbital velocities are lower for GEO and objects are orbiting in the same direction, relative velocities are generally more benign for the GEO regime. Thus, according to Equation (5), although fewer fragments will be generated for a collision event at GEO than for an equivalent event at LEO, peak risk potential increases as a result of a smaller-mean

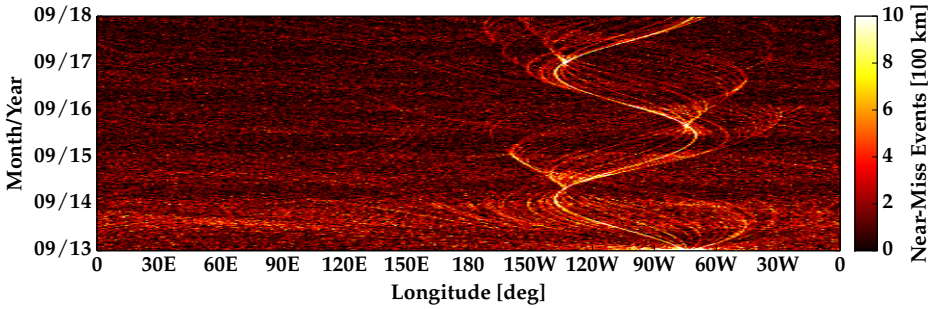


(a) Five-year congestion forecast for simulated R/B explosion at 75°W ($\tilde{r} = 100$ km).

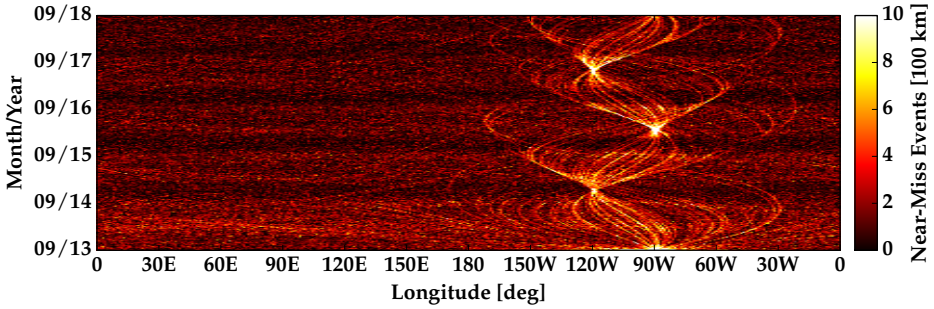


(b) Five-year congestion forecast for simulated R/B explosion at 90°W ($\tilde{r} = 100$ km).

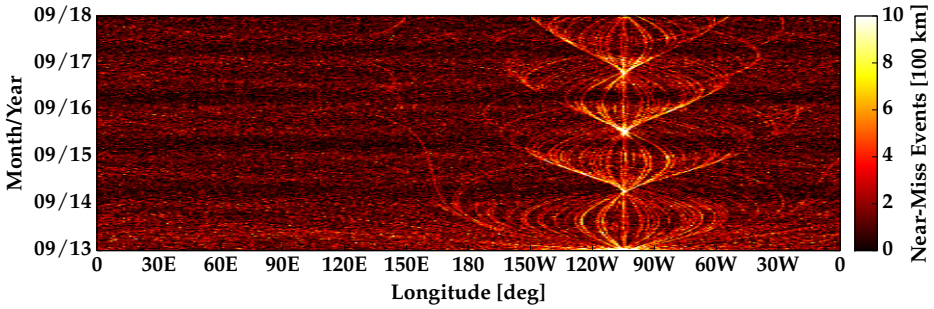


(c) Five-year congestion forecast for simulated R/B explosion at 105°W ($\tilde{r} = 100$ km).

**Figure 7. Longitude-dependent congestion from simulated R/B explosions near Western well.**

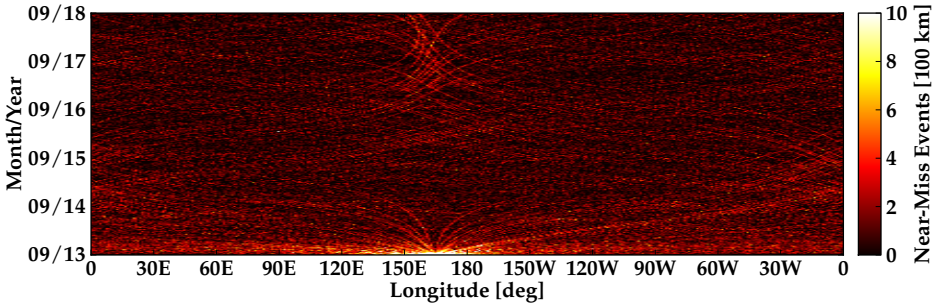


**Figure 8. Five-year congestion forecast for simulated R/B explosion at 165°E ($\tilde{r} = 100$ km).**

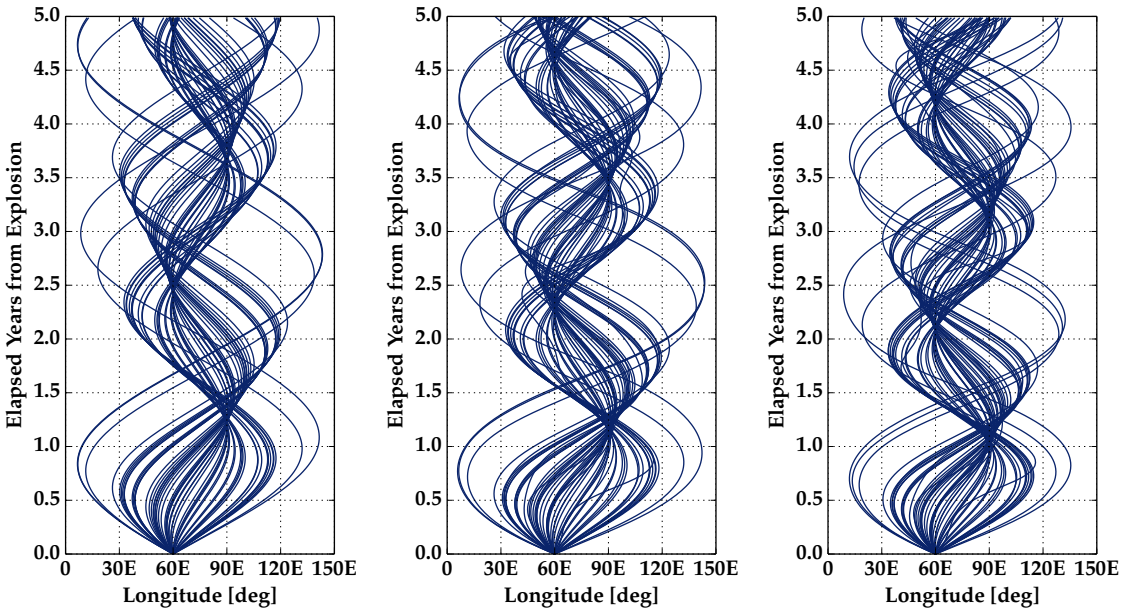


(a) Harmonic oscillator approximation. (b) Longitude histories ($J_{2,2}$ only). (c) Longitude histories (full forcing).

**Figure 9. Accuracy of harmonic oscillator model for predicting longitudes of librating fragments.**

fragmentation $\Delta v$ distribution.[8] For this study, three collision events over the Eastern gravity well are simulated: (a) collision due to inclination difference, (b) collision due to eccentricity difference, and (c) collision between objects in GEO and geostationary transfer (GTO) orbits. For all scenarios, two 2000 kg upper stages are assumed to collide at 60°E, using the initial conditions of the "target" R/B implemented for the explosion cases shown earlier in this paper. Simulation results are given in Table 2, and the five-year congestion forecasts for each collision scenario are presented in Figure 10.

**Table 2. Simulation results for three collision scenarios between two 2000 kg upper stages at 60°E.**

| Case | Collision Case Description | Collision Speed | $N_f$ (Capt.) |
|---|---|---|---|
| I | Collision with inclination difference $\Delta i = 2.0°$ | 0.107 km/s (NC) | 941 (61) |
| II | Collision with eccentricity difference $\Delta e = 0.05$ | 0.157 km/s (NC) | 1251 (71) |
| III | Collision at apogee of 200 km × 35744 km GTO | 1.479 km/s (C) | 8439 (218) |

The first two simulated collisions are non-catastrophic according to the specific energy defined in Equation (6), and a smaller proportion of fragments are captured by the gravitational well for both of these cases than for the 60°E explosion case (6.5% and 5.7% are captured for the inclination and eccentricity difference collision events, respectively, compared to the 8.3% captured in the explosion case). This is largely a consequence of the fragmentation velocity distribution in the NASA Standard Breakup Model, which defines a higher mean $\Delta v$ for collision events than for explosion events.[10] In the third simulated collision event, defined as catastrophic according to Equation (6), a mere 2.6% of the staggering 8439 fragments larger than 5 cm in diameter are captured by the gravitational well.

Figure 10 shows that the localized congestion forecasts generated by collision events qualitatively

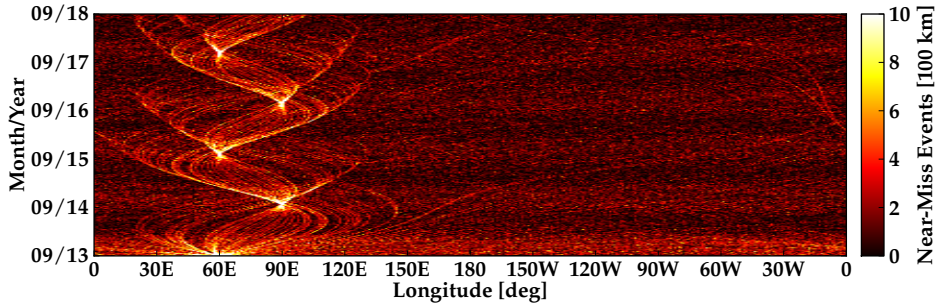


(a) Five-year congestion forecast for simulated collision at 60°E (inclination difference).

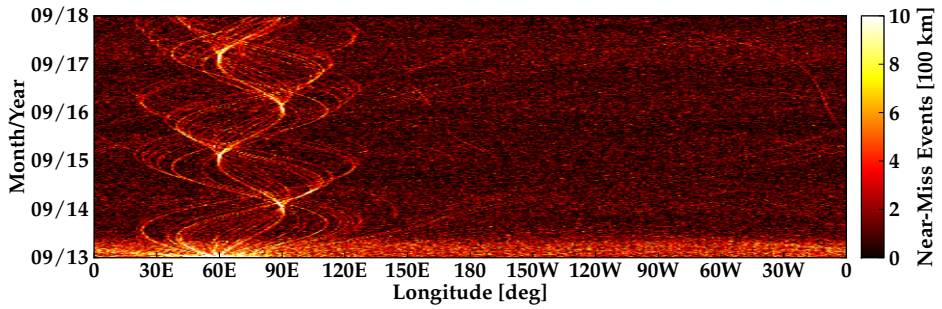


(b) Five-year congestion forecast for simulated collision at 60°E (eccentricity difference).

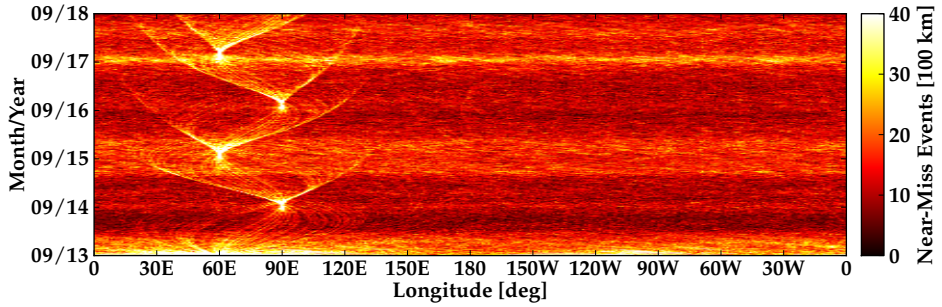


(c) Five-year congestion forecast for simulated collision at 60°E (GEO-GTO apogee collision).

**Figure 10. Longitude-dependent congestion from simulated R/B collisions near Eastern well.**

appear to be very similar to the macroscopic trends exhibited by explosion events, even though two separate fragment clouds exist in the former, and only a single ejecta cloud is generated in the latter. The significant increase in the number of near-miss events at 100 km for the GEO-GTO collision in Figure 10(c) is a consequence of the large number of fragments ejected in this catastrophic collision only. Longitudinal bunching at the libration amplitude of the "target" R/B is still observed at similar periodicity in all three collision scenarios, although localized congestion during a bunching event in Figure 10(c) is a factor of four times more intense than for the inclination and eccentricity difference cases in Figures 10(a)-10(b). These results indicate that the longitude-dependent effects of explosion and collision events in the GEO ring are equivalent in characteristic, and differ strictly by the number of fragments that are captured by the gravitational well for each scenario (cf. Figures 4(b) and 10).

## CONCLUSIONS

The effect of on-orbit fragmentation events on longitude-dependent debris congestion in the GEO regime is investigated by simulating explosions and collisions of uncontrolled rocket bodies in various orbit configurations, including libration about one or both of the critical E/W stable longitudes at the GEO altitude. Using the NASA Standard Breakup Model in tandem with the torus intersection metric and parallel propagation routine, both short- and long-term localized congestion patterns are rapidly forecasted to investigate how strongly the severity of the fragmentation event depends upon the longitude of the parent body at the epoch of fragmentation. Simulation results indicate that on-orbit fragmentations in the vicinity of one of the critical gravitational wells spawn bi-annual debris storms at the longitudinal extents of the parent body's libration motion. Provided the delta-velocity distribution for the GEO fragmentation can be reasonably estimated using tracking data, longitudes and times at which dramatic increases in congestion will occur can be predicted to first-order, using the presented harmonic oscillator formulation for time frames of less than five elapsed years. In all fragmentation scenarios, the level of TLE background noise was achieved or surpassed only during the observed longitudinal bunching events: the intensity of these debris storms is proportional to the number of particles captured by the gravitational well, however, and therefore may readily overtake background congestion levels if higher-energy collisions are considered (as in the scenario of a GTO apogee collision), or if effective fragment diameters smaller than 5 cm are included. Ultimately, this study highlights the importance of energy passivation at end-of-life – satellites and upper stages that are not properly prepared during decommissioning operations are prone to fragmenting and creating a debris cloud that has threatening and expensive consequences for operational assets in this regime.

## ACKNOWLEDGMENT

The authors would like to acknowledge the U.S. Department of Defense and the National Defense Science and Engineering Graduate Fellowship (NDSEG), the program through which funding for this research was obtained. The authors furthermore acknowledge Brandon Jones and the TurboProp software suite,[30] from which the integration routines employed in this research were obtained.

## REFERENCES

[1] N. Johnson, "Protecting the GEO Environment: Policies and Practices," *Space Policy*, Vol. 15, 1999, pp. 127–135.

[2] R. Jehn, V. Agapov, and C. Hernandez, "The Situation in the Geostationary Ring," *Advances in Space Research*, Vol. 35, 2005, pp. 1318–1327.

[3] P. Chrystal, D. McKnight, and P. Meredith, "Space Debris: On Collision Course for Insurers?," tech. rep., Swiss Reinsurance Company Ltd, 2011.

[4] H. Klinkrad, *Space Debris: Models and Risk Analysis*. Praxis Publishing, 2006.

[5] T. Schildknecht, M. Ploner, and U. Hugentobler, "The Search for Debris in GEO," *Advances in Space Research*, Vol. 28, No. 9, 2001, pp. 1291–1299.

[6] T. Schildknecht, R. Musci, M. Ploner, G. Beutler, W. Flury, J. Kuusela, J. d. Leon Cruz, and L. d. Fatima Dominguez Palmero, "Optical Observations of Space Debris in GEO and in Highly-Eccentric Orbits," *Advances in Space Research*, Vol. 34, 2004, pp. 901–911.

[7] D. S. McKnight, *Simulation of On-Orbit Satellite Fragmentations*. PhD thesis, University of Colorado at Boulder, 1986.

[8] B. W. Hansen and M. E. Sorge, "Summarizing the General Effects of Breakup Debris in GEO," *Proceedings of the 2013 AAS/AIAA Astrodynamics Specialist Conference*, No. 13-844, August 2013.

[9] P. V. Anderson and H. Schaub, "Local Orbital Debris Flux Study in the Geostationary Ring," *Advances in Space Research*, Vol. 51, June 2013, pp. 2195–2206, http://dx.doi.org/10.1016/j.asr.2013.01.019.

[10] N. L. Johnson, P. H. Krisko, J.-C. Liou, and P. D. Anz-Meador, "NASA's New Breakup Model of Evolve 4.0," *Advances in Space Research*, Vol. 28, No. 9, 2001, pp. 1377–1384.

[11] T. Yasaka and N. Ishii, "Breakup in Geostationary Orbit: A Possible Creation of a Debris Ring," *Acta Astronautica*, Vol. 26, No. 7, 1992, pp. 523–530.

[12] D. Oltrogge and D. Finkleman, "Consequences of Debris Events in Geosynchronous Orbit," *Proceedings of the 2008 AIAA/AAS Astrodynamics Specialist Conference and Exhibit*, No. 2008-7375, August 2008.

[13] H. Curtis, *Orbital Mechanics for Engineering Students*. Elsevier Butterworth-Heinemann, 2005.

[14] D. Vallado, *Fundamentals of Astrodynamics and Applications*. Microcosm Press, 3 ed., 2007.

[15] O. Montenbruck and E. Gill, *Satellite Orbits: Models, Methods, Applications*. Springer, 2000.

[16] H. Schaub and L. E. Z. Jasper, "Circular Orbit Radius Control using Electrostatic Actuation for 2-Craft Configurations," *Proceedings of the 2011 AAS/AIAA Astrodynamics Specialist Conference*, August 2011.

[17] USNO and UKHO, *The Astronomical Almanac for the Year 2013*. U. S. Nautical Almanac Office with Her Majesty's Nautical Almanac Office, 2013.

[18] P. V. Anderson and H. Schaub, "Local Debris Congestion in the Geosynchronous Environment with Population Augmentation," *Acta Astronautica*, Vol. 94, February 2014, pp. 619–628, `http://dx.doi.org/10.1016/j.actaastro.2013.08.023`.

[19] M. M. Berry and L. M. Healy, "Implementation of Gauss-Jackson Integration for Orbit Propagation," *Journal of the Astronautical Sciences*, Vol. 52, July-September 2004, pp. 331–357.

[20] T. Flohrer, "Classification of Geosynchronous Objects: Issue 15," Tech. Rep. 1, European Space Operations Centre, February 2013.

[21] F. R. Hoots and R. L. Roehrich, "Spacetrack Report No. 3: Models for Propagation of NORAD Element Sets," tech. rep., Office of Astrodynamics, Aerospace Defense Center, December 1980.

[22] D. A. Vallado, P. Crawford, R. Hujsak, and T. S. Kelso, "Revisiting Spacetrack Report No. 3: Revision 2," *Proceedings of the 2006 AIAA/AAS Astrodynamics Specialist Conference*, August 2006.

[23] P. Wegener, J. Bendisch, H. Krag, M. Oswald, and S. Stabroth, "Population Evolution in the GEO Vicinity," *Advances in Space Research*, Vol. 34, 2004, pp. 1171–1176.

[24] K. Luu and C. Sabol, "Effects of Perturbations on Space Debris in Supersynchronous Storage Orbits," tech. rep., Air Force Research Laboratory, October 1998.

[25] V. A. Chobotov, ed., *Orbital Mechanics*. American Institute of Aeronautics and Astronautics, Inc., 3 ed., 2002.

[26] D. S. McKnight and F. R. Di Pentino, "New Insights on the Orbital Debris Collision Hazard at GEO," *Acta Astronautica*, Vol. 85, 2013, pp. 73–82.

[27] R. R. Allan, "Perturbations of a Geostationary Satellite by the Longitude-Dependent Terms in the Earth's Gravitational Field," *Planetary and Space Science*, Vol. 11, August 1963, pp. 1325–1334.

[28] C.-C. Chao, *Applied Orbit Perturbation and Maintenance*. The Aerospace Press, 2005.

[29] S. Jones, "Negating the Yearly Eccentricity Magnitude Variation of Super-synchronous Disposal Orbits due to Solar Radiation Pressure," Master's thesis, University of Colorado at Boulder, 2013.

[30] K. Hill and B. A. Jones, *TurboProp Version 4.0*. Colorado Center for Astrodynamics Research, University of Colorado at Boulder, May 2009.